OPEN ACCESS
CellPress

Cell Reports
Report

Role of Angiopoietin-2 in Adaptive Tumor Resistance to VEGF Signaling Blockade

Nicolò Rigamonti,[1,3] Ece Kadioglu,[1,3] Ioanna Keklikoglou,[1] Céline Wyser Rmili,[1] Ching Ching Leow,[2] and Michele De Palma[1,*]

[1]Swiss Institute for Experimental Cancer Research (ISREC), School of Life Sciences, École Polytechnique Fédérale de Lausanne (EPFL), 1015 Lausanne, Switzerland

[2]Translational Medicine Oncology, MedImmune, Gaithersburg, MD 20878, USA

[3]Co-first author

*Correspondence: michele.depalma@epfl.ch

http://dx.doi.org/10.1016/j.celrep.2014.06.059

SUMMARY

Angiopoietin-2 (ANG2/ANGPT2) is a context-dependent TIE2 receptor agonist/antagonist and proangiogenic factor. Although ANG2 neutralization improves tumor angiogenesis and growth inhibition by vascular endothelial growth factor (VEGF)-A signaling blockade, the mechanistic underpinnings of such therapeutic benefits remain poorly explored. We employed late-stage RIP1-Tag2 pancreatic neuroendocrine tumors (PNETs) and MMTV-PyMT mammary adenocarcinomas, which develop resistance to VEGF receptor 2 (VEGFR2) blockade. We found that VEGFR2 inhibition upregulated ANG2 and vascular TIE2 and enhanced infiltration by TIE2-expressing macrophages in the PNETs. Dual ANG2/VEGFR2 blockade suppressed revascularization and progression in most of the PNETs, whereas it had only minor additive effects in the mammary tumors, which did not upregulate ANG2 upon VEGFR2 inhibition. ANG2/VEGFR2 blockade did not elicit increased PNET invasion and metastasis, although it exacerbated tumor hypoxia and hematopoietic cell infiltration. These findings suggest that evasive tumor resistance to anti-VEGFA therapy may involve the adaptive enforcement of ANG2-TIE2 signaling, which can be reversed by ANG2 neutralization.

INTRODUCTION

Tumor growth and progression depend on angiogenesis, the formation and expansion of intratumoral blood vessels. Among the positive regulators of tumor angiogenesis are the vascular endothelial growth factor (VEGF)-A and its endothelial cell (EC)-specific tyrosine kinase receptor, VEGF receptor 2 (VEGFR2) (Chung et al., 2010). However, preclinical studies in mice show that several tumor models are refractory or rapidly develop resistance to VEGFA/VEGFR2-targeting drugs (Bergers and Hanahan, 2008; Vasudev and Reynolds, 2014). Although there is clinical evidence for bevacizumab—a monoclonal antibody (moAb) that neutralizes human VEGFA—to decrease tumor angiogenesis, edema, and/or disease burden when administered as monotherapy (Van der Veldt et al., 2012; Willett et al., 2004; Yang et al., 2003), the survival improvements, also in combination with first-line anticancer drugs, are generally modest (Vasudev and Reynolds, 2014). The failure of VEGF pathway inhibitors to induce durable antitumoral responses mirrors that of other mechanism-targeted drugs (De Palma and Hanahan, 2012) and can be attributed to preexisting or induced compensatory proangiogenic signaling (Casanovas et al., 2005; Shojaei et al., 2008), some of which are conveyed by stromal cells (Bergers and Hanahan, 2008; De Palma and Lewis, 2013; Ferrara, 2010; Rivera et al., 2014). Furthermore, effective inhibition of tumor angiogenesis by anti-VEGFA/VEGFR2 moAbs or kinase inhibitors that also block the VEGFRs (e.g., sunitinib) may evoke forms of tumor adaptation that circumvent the need of angiogenesis, such as cancer growth by increased local invasion and blood vessel co-option (Bergers and Hanahan, 2008; Sennino and McDonald, 2012).

The angiopoietin (ANG)-TIE2 system regulates vascular development and maturation (Eklund and Saharinen, 2013). In the resting vasculature, pericyte-derived ANG1 constitutively binds the TIE2 receptor expressed on ECs to activate AKT signaling and promote EC survival and quiescence. Although angiopoietin-2 (ANG2/ANGPT2) can disrupt ANG1-TIE2 signaling, increasing data indicate that it can also function as a TIE2 agonist, particularly when overexpressed and/or in the absence of ANG1 (Daly et al., 2013; Gerald et al., 2013). In angiogenic tissues like tumors, ECs secrete high levels of ANG2, which operates autocrinally and paracrinally as the main TIE2 ligand to promote angiogenesis in concert with other proangiogenic factors, namely VEGFA (Eklund and Saharinen, 2013). ANG2, but not ANG1, levels are elevated in the plasma of patients with cancer compared to healthy subjects; furthermore, higher circulating ANG2 may correlate with a more advanced stage of the disease and/or a worse prognosis in some cancer types (Helfrich et al., 2009; Park et al., 2007). Although the mechanisms underlying the divergent vascular responses triggered by ANG1 and ANG2 remain poorly defined, different oligomerization states of ANG1 and ANG2 may differentially regulate the subcellular localization of TIE2 or its association with distinct cellular or matrix

coreceptors (Eklund and Saharinen, 2013). Furthermore, ANG2 may modulate the proangiogenic functions of perivascular TIE2-expressing macrophages (TEMs) (Mazzieri et al., 2011).

ANG2 blockade decreases angiogenesis and slows the growth of several tumor models, often more prominently so when combined with VEGFA/VEGFR2 inhibitors (Brown et al., 2010; Daly et al., 2013; Hashizume et al., 2010; Holopainen et al., 2012; Huang et al., 2011; Kienast et al., 2013; Leow et al., 2012; Mazzieri et al., 2011). However, it is unclear whether ANG2-TIE2 signaling may sustain VEGF-independent angiogenesis in tumor models that are refractory or acquire resistance to VEGFA/VEGFR2-targeted drugs. For example, late-stage pancreatic neuroendocrine tumors (PNETs) that develop in RIP1-Tag2 mice revascularize following a transient response phase to VEGFA signaling blockade, a phenomenon associated with the compensatory upregulation of basic fibroblast growth factor 2 (FGF2) (Allen et al., 2011; Casanovas et al., 2005). Here, we employed two mouse tumor models, RIP1-Tag2 PNETs and MMTV-PyMT mammary adenocarcinomas, to investigate the putative role of ANG2 in adaptive tumor resistance to VEGFR2 blockade.

RESULTS

Combined ANG2/VEGFR2 Inhibition Blocks Revascularization and Progression of Late-Stage PNETs in RIP1-Tag2 Mice

We first studied ANG2/VEGFR2 blockade in late-stage PNETs of RIP1-Tag2 mice. We analyzed tumor growth and angiogenesis on pancreatic sections by anti-SV40 large T antigen (TAg) immunostaining (to identify TAg^+ PNETs), anti-CD31/PECAM1 immunostaining (to identify blood vessels), and/or after in vivo fluorescein isothiocyanate (FITC)-lectin perfusion and direct FITC visualization (to identify functional blood vessels).

We found that three consecutive doses (administered every 3.5 days) of either 0.5 or 1.0 mg of the anti-VEGFR2 moAb DC101 (Prewett et al., 1999) effectively and comparably decreased PNET vascularization by more than 60% in male RIP1-Tag2 mice treated starting at 12 weeks of age (versus rat immunoglobulin G [IgG] control [R.IgG]; Figure 1A). We therefore selected 0.5 mg DC101 per mouse given biweekly as the lower effective biological dose for further studies. We then treated 11.5- to 12.5-week-old male RIP1-Tag2 mice with biweekly injections of DC101, 3.19.3 (an anti-ANG2 moAb; Brown et al., 2010), the combination of the two (DC101 plus 3.19.3), or the appropriate IgG controls (R.IgG for DC101, human IgG [H.IgG] for 3.19.3, or the combination of the two [R plus H.IgG]), according to an extended treatment schedule (seven to eight consecutive doses for 3.5–4.0 weeks). We also treated a group of mice with three doses of DC101 followed by four doses of DC101 plus 3.19.3. We euthanized the treated mice at 15.0–16.0 weeks of age, which coincides with end-stage disease in this genetically engineered mouse model (GEMM) of cancer, or untreated mice at 12 weeks of age, in order to obtain pancreata at the initiation of therapy (t_0).

The total pancreatic tumor area was similar in DC101 and control IgG-treated mice (Figures 1B and 1C), indicating unaltered tumor progression under VEGFR2 blockade despite the initial antiangiogenic response. Likewise, 3.19.3 monotherapy had minimal effects on tumor progression. Conversely, DC101 plus 3.19.3-treated mice had a significantly smaller tumor area compared to mice treated with monotherapies or control IgGs. Of note, the pancreatic tumor area was indistinguishable from that at t_0, indicating that on average, DC101 plus 3.19.3-treated PNETs had not progressed since the t_0. The combination of DC101 and 3.19.3 was effective also when it was started after a short treatment schedule with DC101 monotherapy.

We then analyzed the pancreata by their gross appearance and found that those of DC101 plus 3.19.3-treated mice had exceedingly fewer hemorrhagic/vascularized tumors than those in the other groups (Figures 1D and S1A). To investigate this further, we analyzed tumor vascularization microscopically. Both DC101 and 3.19.3 administered singly decreased, albeit moderately, the relative $CD31^+$ vascular area compared to control IgGs (by ~30% and 20%, respectively; Figure 1E). The relative vascular area in DC101-treated tumors had therefore increased compared to that at 1.5 weeks posttreatment (Figure 1A), a manifestation of adaptive resistance to antiangiogenic therapy (Casanovas et al., 2005). Of note, the combination of DC101 and 3.19.3 was much more effective than either alone and dramatically abated the proportion of PNETs with relatively high vascular area.

The tumor blood vessels differed qualitatively among the different treatment groups (Figure 1F). Control IgG-treated tumors displayed a dense vascular network, made of highly branched and heterogeneous vessels. Whereas DC101 did not appreciably modify the morphology of the blood vessels, those in 3.19.3-treated tumors were frequently more enlarged and less branched than in control IgG or DC101-treated tumors. Remarkably, DC101 plus 3.19.3 produced large avascular tumor areas (Figure S1B), suggesting that both inhibition of angiogenesis and vascular regression had occurred. In these tumors, the blood vessels were mostly located at the tumor periphery, were poorly branched, had a small diameter, and displayed enhanced coverage by neural-glial 2 $(NG2)^+$ pericytes compared to those of control tumors (Figures 1G and 1H). The latter phenotype was possibly an anti-ANG2-mediated dominant effect because 3.19.3 induced a similar phenotype, in agreement with previous observations by Holopainen et al. (2012) and Mazzieri et al. (2011). Unlike DC101 monotherapy, both 3.19.3 and DC101 plus 3.19.3 reduced the relative $lectin^+$ area compared to the controls (Figures 1I and S1C). The latter findings suggest that DC101 preferentially inhibits or prunes immature (nonperfused) blood vessels, whereas 3.19.3, or its combination with DC101, also targets more mature (perfused) blood vessels.

We obtained similar results in T and B cell-deficient *Rag1*$^{-/-}$/RIP1-Tag2 mice, indicating that the antiangiogenic effects of ANG2/VEGFR2 blockade by 3.19.3 and DC101 are largely independent of the adaptive immune system (Figures 1I and S1A). Collectively, the aforementioned data indicate that ANG2 blockade effectively limits rebound angiogenesis following VEGF signaling blockade in PNETs.

ANG2/VEGFR2 Blockade Increases PNET Hypoxia and Hematopoietic-Cell Infiltration without Eliciting Increased Invasion and Metastasis in RIP1-Tag2 Mice

Efficient angiogenesis inhibition and/or vascular pruning by antiangiogenic drugs may exacerbate tumor hypoxia (Bergers and

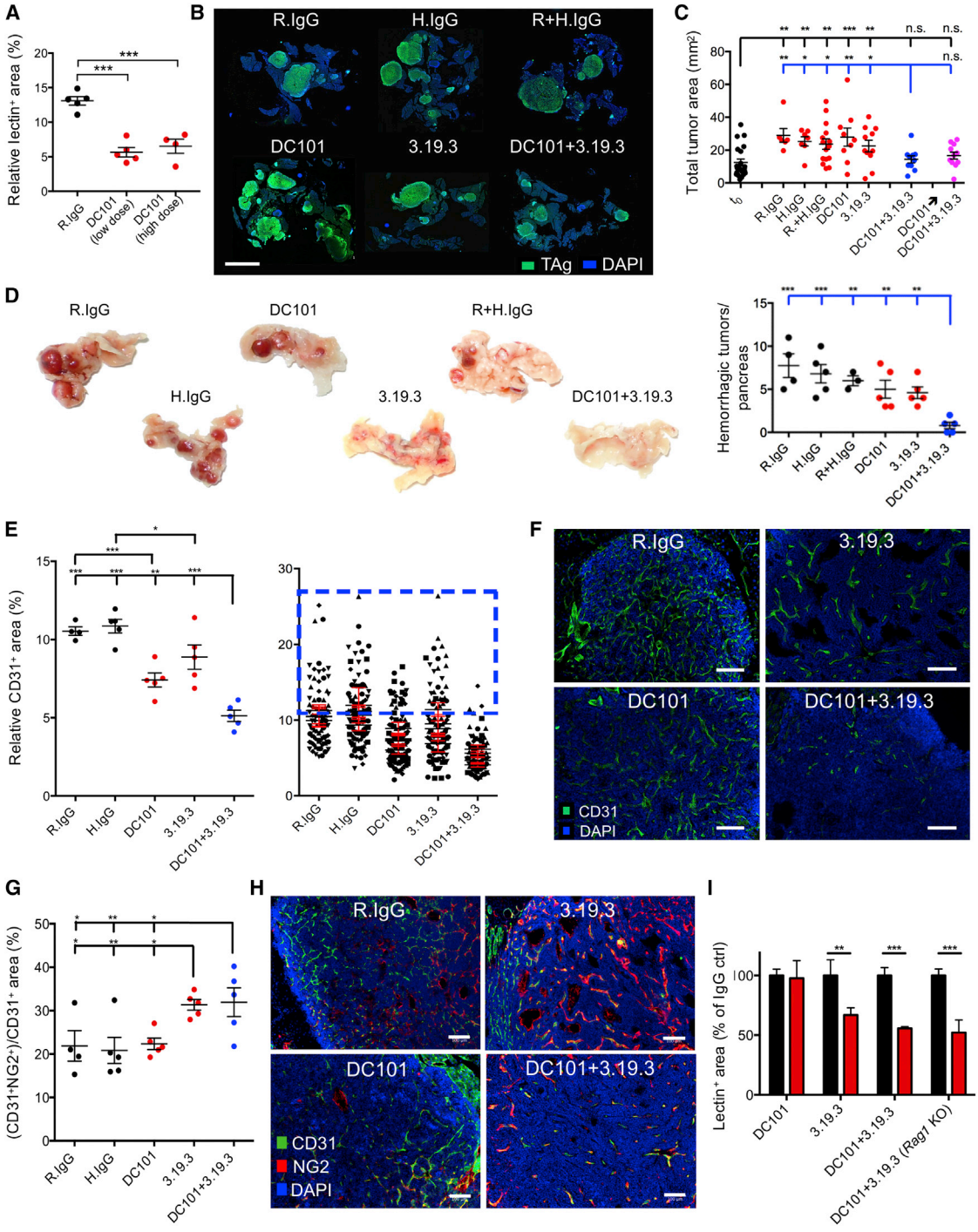

Figure 1. ANG2/VEGFR2 Blockade Abates PNET Progression and Angiogenesis in RIP1-Tag2 Mice

(A) Relative lectin$^+$ vascular area (mean ± SEM) in PNETs treated for 1.5 weeks as indicated: R.IgG (n = 5 mice), low-dose DC101 (n = 5), and high-dose DC101 (n = 4). Each dot represents one mouse, of which multiple tumors were analyzed. Statistical analysis was performed by unpaired two-tailed Student's t test.

(B) Representative images of TAg (green) immunostaining and DAPI (blue) nuclear staining of whole-pancreatic sections from mice treated as indicated. Scale bar, 3 mm.

(C) Total tumor area (mean ± SEM) in the largest pancreatic section of mice treated as indicated: t_0 (n = 21 mice), R.IgG (n = 6), H.IgG (n = 7), R+H.IgG (n = 15), DC101 (n = 9), 3.19.3 (n = 11), DC101+3.19.3 (n = 10), and DC101 followed by DC101+3.19.3 (n = 11). Each dot represents one mouse. Statistical analysis was performed by one-way ANOVA with multiple comparison Fisher's LSD test. n.s., not significant.

(D) Left: representative images of whole pancreata from mice treated as indicated. Right panel shows the number of hemorrhagic PNETs (mean ± SEM) in each pancreas. Each dot represents one mouse. Statistical analysis was performed as in (C).

(legend continued on next page)

Hanahan, 2008; Sennino and McDonald, 2012). Hypoxia was uneven, albeit prevalently low, in control PNETs (Figure 2A), consistent with adequate tumor perfusion by the rich vascular network. DC101-treated tumors were more hypoxic than the controls, but the degree of hypoxia was remarkably uneven, ranging from nonhypoxic to highly hypoxic regions, the latter often surrounding hemorrhagic/necrotic tumor areas. Consistent with their poor vascularization, DC101 plus 3.19.3-treated tumors were uniformly and highly hypoxic.

Previous studies have shown that antiangiogenesis-induced hypoxia may increase tumor invasion and metastasis (Bergers and Hanahan, 2008; Sennino and McDonald, 2012). We then analyzed PNET invasiveness as previously described by Pàez-Ribes et al. (2009). Although being highly hypoxic, DC101 plus 3.19.3-treated tumors did not display increased invasiveness compared to the other experimental groups, as shown by the similar frequency of noninvasive (IC0), microinvasive (IC1), and widely invasive (IC2) PNETs (Figure 2B). Furthermore, we did not detect obvious, treatment-dependent effects on the incidence of liver micrometastases (Table S1; Figures S2A and S2B). These observations suggest that angiogenesis inhibition in DC101 plus 3.19.3-treated PNETs leads to a chronically hypoxic tumor state, which impedes tumor growth but does not elicit heightened invasion or metastasis.

Vascular-targeted therapies may also enhance tumor infiltration by proangiogenic cells through both hypoxia-dependent and -independent mechanisms (De Palma and Lewis, 2013; Ferrara, 2010; Rivera et al., 2014). We found that DC101 plus 3.19.3 increased tumor infiltration by $CD45^+$ hematopoietic cells (Figures 2C and 2D)—the vast majority of which were macrophages (Figure 2E)—compared to the other treatment groups. Because the extent of tumor infiltration by $CD45^+$ cells correlated with tumor vascularization in both DC101 plus 3.19.3 and control IgG-treated PNETs (Figure 2F), it is conceivable that therapy-induced, de novo recruitment of hematopoietic cells/macrophages may have contributed to limit—at least to some degree—the antiangiogenic and tumor-suppressive effects of ANG2/VEGFR2 blockade in RIP1-Tag2 mice.

VEGFR2 Blockade Upregulates ANG2 and TIE2 in the PNETs of RIP1-Tag2 Mice

We then sought to investigate the molecular events underlying the synergistic antiangiogenic and antitumoral effects of double ANG2/VEGFR2 blockade in the PNETs. To this aim, we first dissected and classified individual tumors as either hemorrhagic/red (R) or nonhemorrhagic/whitish (W) based on their appearance under a stereomicroscope. Virtually all the PNETs in control IgG-treated mice and the vast majority in either DC101 or 3.19.3-treated mice were R. On the contrary, only a small minority of the tumors were classified so in DC101 plus 3.19.3-treated mice (Figures 1D and S1A; data not shown). Quantitative PCR (qPCR) analysis of the EC-specific gene VE-Cadherin (*Cdh5*) showed that the R and W categories fairly distinguished PNETs with relatively high and low abundance of vascular ECs, respectively (Figure S3A).

We found that DC101-treated tumors had significantly upregulated *Angpt2* transcript levels specifically in the R samples compared to the W samples or IgG-treated tumors (Figures 3A and S3B), possibly through a hypoxia-mediated mechanism (Figure S3C). When normalized to the mean vascular area fraction (see Figure 1E), *Angpt2* transcript levels were, on average, ~2.5 higher in the R DC101 than IgG-treated tumors (Figure 3A), a finding confirmed by ELISA of ANG2 protein (Figure 3B). Of note, circulating ANG2 levels did not increase in the plasma of DC101-treated mice (Figure S3D). We found that DC101 also upregulated *Fgf2* in the R samples compared to IgG-treated tumors (Figure S3E), as reported previously by Casanovas et al. (2005).

Whereas ANG2 is restricted to ECs (Goede et al., 2010), TIE2 is expressed in tumors by both ECs and perivascular macrophages (Eklund and Saharinen, 2013; Mazzieri et al., 2011). When normalized to mean vascular area fraction values, the qPCR data showed a trend toward increased *Tek* transcript levels in R DC101 versus control IgG-treated PNETs (Figure 3C). Because ligand bioavailability and other ill-defined factors may control the trafficking and turnover of the TIE2 receptor posttranscriptionally (Eklund and Saharinen, 2013), we also analyzed TIE2 protein expression in blood vessels and macrophages by immunostaining. Although TIE2 expression was heterogeneous in the blood vessels, the relative $TIE2^+$ vascular area was significantly higher in DC101-treated than control tumors (Figures 3D and 3E). Moreover, DC101 increased the proportion of TEMs among the total $CD45^+$ hematopoietic cells (Figures 3F and 3G), in agreement with recent studies in other tumor models (Gabrusiewicz et al., 2014). Taken together, these findings indicate that VEGFR2 blockade adaptively upregulated both ANG2 and TIE2 expression in late-stage PNETs, possibly to reinforce autocrine and/or paracrine ANG2-TIE2 signaling in ECs and TEMs.

Minor Additive Effects of ANG2/VEGFR2 Blockade in the Absence of ANG2 Upregulation in MMTV-PyMT Mammary Tumors

Human breast cancers are poorly sensitive to anti-VEGFA therapy (Vasudev and Reynolds, 2014). We then asked whether ANG2 blockade could improve the antitumoral activity of DC101 in MMTV-PyMT mammary adenocarcinomas growing orthotopically in syngenic mice (Mazzieri et al., 2011). DC101

(E) Relative $CD31^+$ vascular area (mean ± SEM) in PNETs treated as indicated: R.IgG (n = 4 mice), H.IgG (n = 5), DC101 (n = 5), 3.19.3 (n = 5), and DC101+3.19.3 (n = 5). In the left panel, each dot represents one mouse. In the right panel, each dot represents a tumor image acquired at 200× magnification; the dashed blue box indicates individual values greater than the mean value in R/H.IgG control groups. Statistical analysis was performed as in (C).

(F and H) Representative images of CD31 (green) and NG2 (red) immunostaining and DAPI nuclear (blue) staining of PNETs treated as indicated. Scale bars, 100 μm.

(G) Relative area of pericyte ($NG2^+$)-covered blood vessels in PNETs treated as indicated: R.IgG (n = 4 mice), H.IgG (n = 5), DC101 (n = 5), 3.19.3 (n = 5), and DC101+3.19.3 (n = 5). Each dot represents one mouse, of which multiple tumors were analyzed. Statistical analysis was performed as in (C).

(I) $Lectin^+$ area normalized to IgG control (ctrl; black bars) (mean values ± SEM) in PNETs treated as indicated: DC101 (n = 3 mice), 3.19.3 (n = 4), DC101+3.19.3 (n = 5), DC101+3.19.3, *Rag1* knockout (KO) (n = 6), R.IgG (n = 2), H.IgG (n = 3), R+H.IgG (n = 11), and R+H.IgG, *Rag1* KO (n = 5). For each mouse, multiple tumors were analyzed. Statistical analysis was performed as in (A).

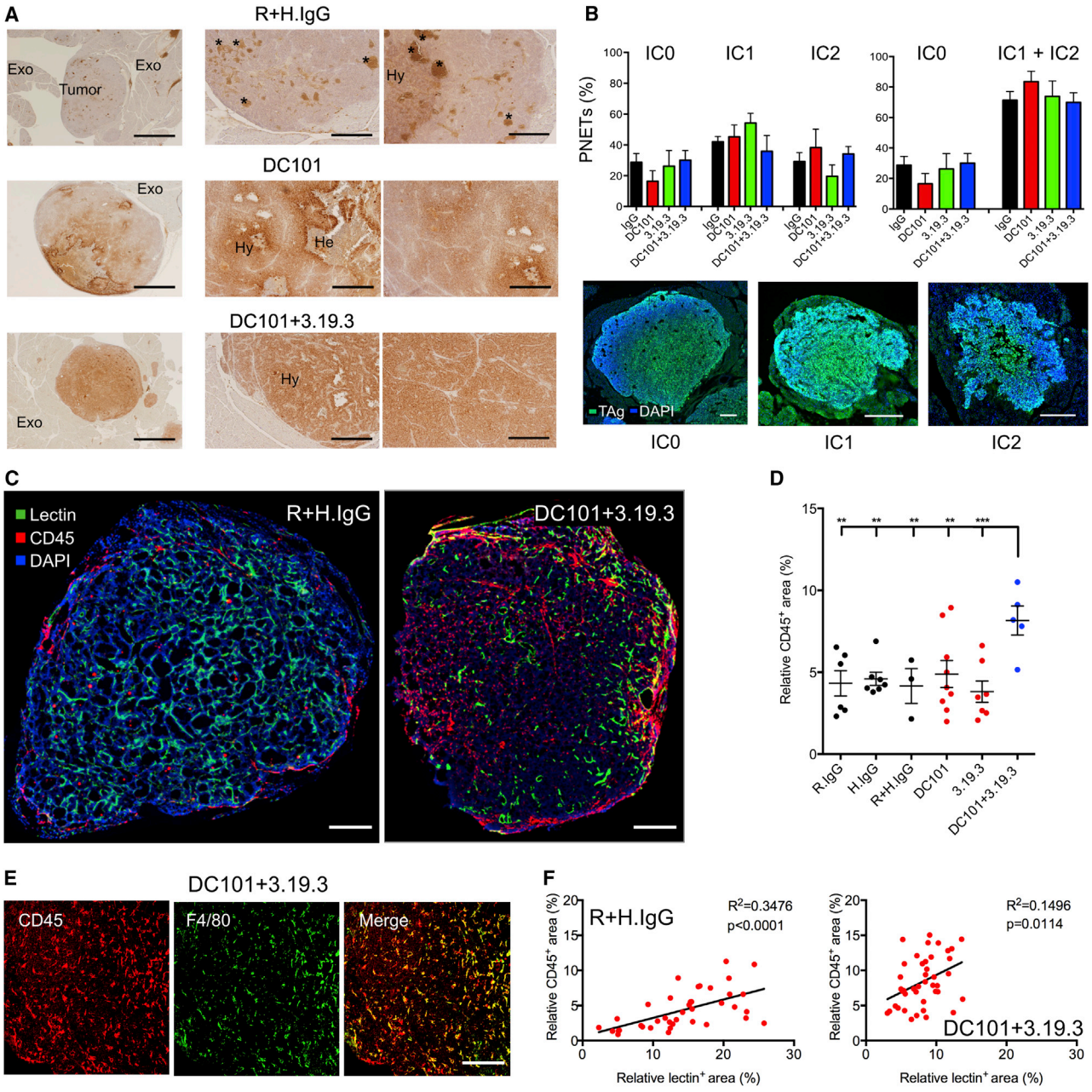

Figure 2. ANG2/VEGFR2 Blockade Increases PNET Hypoxia and Hematopoietic-Cell Infiltration, but Not Local Invasion, in RIP1-Tag2 Mice

(A) Representative images of PNETs treated as indicated (R+H.IgG, n = 3 mice; DC101, n = 3; and DC101+3.19.3, n = 3) and stained with an anti-PIMO moAb (brown) to reveal hypoxia. Scale bars, 1 mm (left images) and 200 μm (middle and right images). Exo, exocrine pancreatic tissue; Hy, hypoxia; He, hemorrhagic/necrotic tissue. Asterisks indicate blood vessels/islands decorated unspecifically by the secondary Ab.

(B) Top panels present quantification of tumor invasion shown as the percentage (mean ± SEM) of IC0, IC1, and IC2 PNETs treated as indicated: R.IgG, H.IgG, or R+H.IgG (IgG) (n = 13 mice, 115 tumors); DC101 (n = 5 mice, 44 tumors); 3.19.3 (n = 5 mice, 36 tumors); and DC101+3.19.3 (n = 5 mice, 46 tumors). No significant differences were found by one-way ANOVA with multiple comparison Fisher's LSD test. Bottom panels show representative images of IC0, IC1, and IC2 PNETs stained as in Figure 1B. Scale bars, 200 μm.

(C) Lectin (green) and CD45 (red) immunostaining and DAPI nuclear (blue) staining of PNETs treated as indicated. Scale bars, 300 μm.

(D) Relative area of $CD45^+$ cells in PNETs treated as indicated: R.IgG (n = 6 mice), H.IgG (n = 7), R+H.IgG (n = 3), DC101 (n = 9), 3.19.3 (n = 7), and DC101+3.19.3 (n = 5). Each dot represents one mouse, of which multiple tumors were analyzed. The data show two independent experiments combined. Statistical analysis was performed as in Figure 1C.

(E) F4/80 (green) and CD45 (red) immunostaining of a representative PNET treated as indicated. Scale bar, 100 μm.

(F) Correlation between the relative $lectin^+$ and $CD45^+$ area in individual PNETs treated as indicated: R+H.IgG (n = 3 mice) and DC101+3.19.3 (n = 4). Each dot represents one tumor. Statistical analysis was performed by Spearman's rank correlation test.

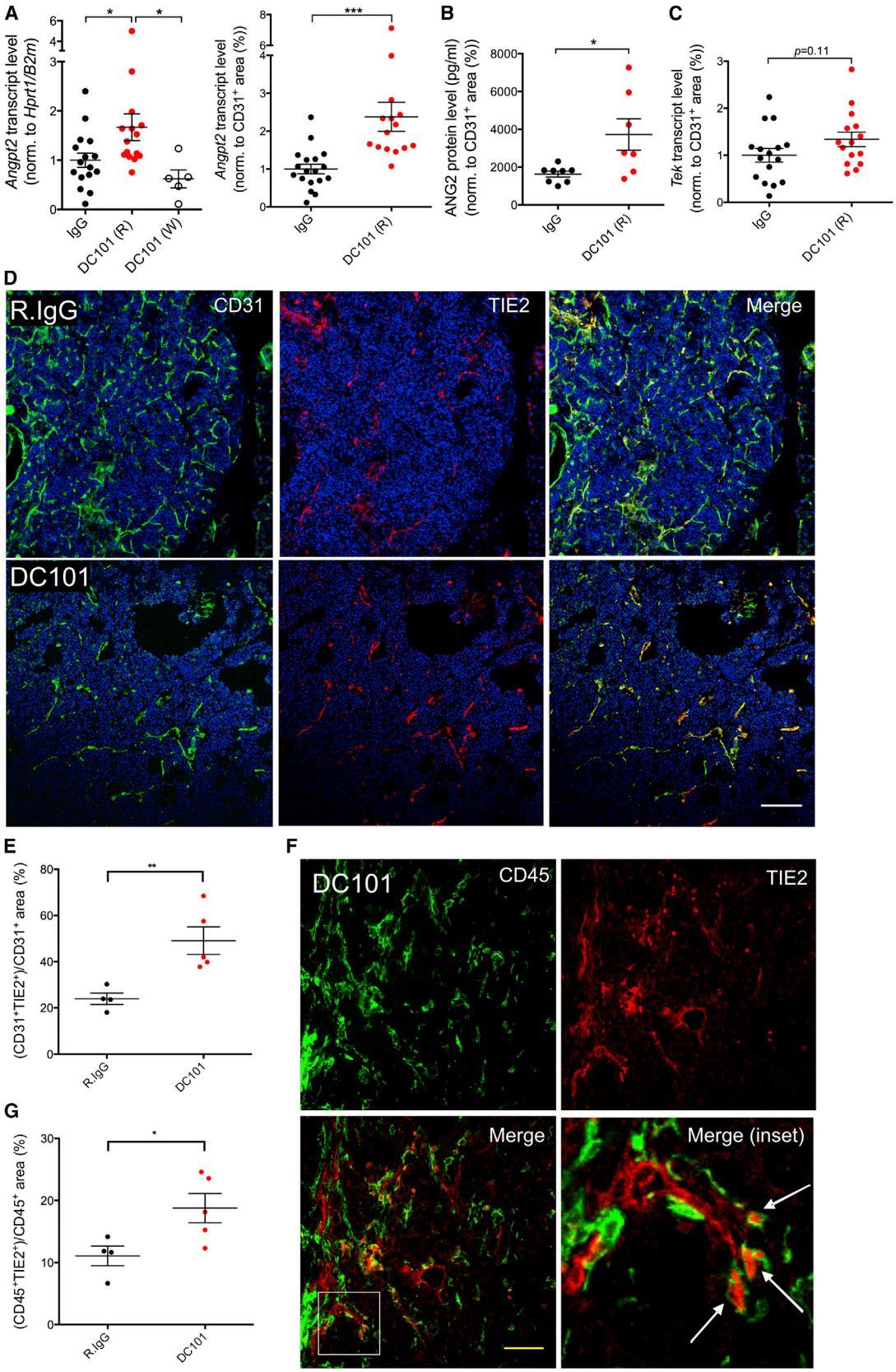

(legend on next page)

inhibited the growth and decreased angiogenesis of established tumors more effectively than 3.19.3 (Figures 4A and 4B). However, evasive resistance to DC101 became apparent after an initial response phase (Figure 4C). ANG2 blockade delayed the emergence of evasive resistance to DC101 but did not produce disease stabilization and hardly had additive antiangiogenic effects compared to DC101 monotherapy (Figure 4D).

We then analyzed the expression of ANG2 and TIE2 in DC101-treated tumors harvested at either early or late stages of the resistance phase. Although VEGFR2 blockade increased *Tek* transcript levels and the proportion of TIE2$^+$ blood vessels in the tumors (Figures S4A and S4B)—similar to the finding in RIP1-Tag2 mice—it did not increase *Angpt2*/ANG2 transcript and protein levels (Figures 4E and 4F). Overall, *Angpt2* transcript levels were significantly lower in the mammary carcinomas than in the PNETs, both at baseline and after DC101 (Figure 4G). Together, these observations suggest a direct association between the lack of upregulation of *Angpt2*/ANG2 levels by DC101 and the lack of synergistic antiangiogenic/antitumoral activities by ANG2/VEGFR2 blockade in MMTV-PyMT mammary carcinomas.

Higher Intratumoral *ANGPT2* Levels May Predict a Worse Response to Bevacizumab-Containing Antiangiogenic Therapy

The aforementioned data suggest that higher intratumoral levels of ANG2 might predict a worse response to VEGFA-targeting therapies, possibly also through routes that are independent of an adaptive mechanism of upregulation. To explore this hypothesis, we analyzed gene expression microarray data from a phase II trial of neoadjuvant bevacizumab and radiotherapy for resectable soft tissue sarcoma (Yoon et al., 2011). In that study, 50% of the patients showed major or complete pathologic responses ($\geq$80% tumor necrosis). We found that higher pretreatment levels of *ANGPT2* were, albeit weakly, associated with a poor response to neoadjuvant therapy (Figure S4C). Because the EC-specific genes *CDH5* and *KDR* (VEGFR2) were not differentially expressed in tumors with a good or bad response, the data suggest that *ANGPT2* may be a predictive biomarker of response to bevacizumab in this tumor type.

DISCUSSION

In this study, we report that (1) evasive resistance to antiangiogenic therapy by VEGFA signaling blockade in RIP1-Tag2 PNETs is associated with the adaptive upregulation of *Angpt2*/ANG2, (2) combined ANG2/VEGFR2 blockade blunts rebound angiogenesis and blocks tumor progression in the vast majority of the PNETs, and (3) the lack of adaptive upregulation of *Angpt2*/ANG2 may lie behind the lack of synergy between VEGFA and ANG2 signaling blockade in MMTV-PyMT mammary carcinomas. Our analysis of published microarray data (Yoon et al., 2011), although limited, further indicates that higher intratumoral levels of *ANGPT2* in nontreated human sarcomas may predict a poor response to bevacizumab-containing neoadjuvant therapy, thus suggesting that elevated ANG2 may curb tumor responsiveness to VEGF neutralization also through a primary resistance/refractoriness mechanism (Bergers and Hanahan, 2008). Together with our findings in mouse tumor models, the aforementioned clinical data may motivate the selection of patients that are more likely to respond to bevacizumab-containing neoadjuvant therapy based on low intratumoral ANG2 levels.

Whereas intratumoral *Angpt2*/ANG2 levels were upregulated, its circulating levels did not increase in DC101-treated RIP1-Tag2 mice, possibly because of the overall low tumor burden in this GEMM of cancer. Recent studies have shown that higher pretreatment levels of plasma/serum ANG2 predict an unfavorable clinical outcome in patients with metastatic colorectal cancer (CRC) treated by bevacizumab in combination with chemotherapy (Goede et al., 2010; Kim et al., 2013). However, these studies did not stratify patients according to disease burden. We found that circulating levels of ANG2 increase proportionally with the tumor burden in transgenic MMTV-PyMT mice (data not shown), in agreement with findings in patients with melanoma (Helfrich et al., 2009). Thus, lower circulating ANG2 levels might mirror a lower disease burden, which may associate with a more favorable clinical outcome in metastatic CRC (Goede et al., 2010; Kim et al., 2013). It remains to be seen whether intratumoral ANG2 levels could predict tumor response to bevacizumab-containing therapies in CRC and, possibly, other cancer types.

A recent study has shown that ANG2 can activate the TIE2 receptor on ECs to protect them from the antiangiogenic effects of VEGF inhibition (Daly et al., 2013). Our findings in RIP1-Tag2 mice not only support those of Daly et al. (2013) but also put forward the concept that VEGFA signaling blockade may adaptively enforce ANG2-TIE2 signaling to promote VEGF-independent tumor angiogenesis. Although it is unclear why MMTV-PyMT mammary carcinomas did not upregulate ANG2 in response to VEGFR2 blockade, it is tempting to speculate that transient vascular pruning and increased tumor hypoxia may have enforced ANG2 transcription and secretion from the remaining blood vessels in the PNETs, thus rescuing angiogenesis. Consistent with this scenario and previous data (Oh et al., 1999), we

Figure 3. VEGFR2 Blockade Upregulates ANG2 and TIE2 in the PNETs of RIP1-Tag2 Mice

(A and C) qPCR-based gene expression analysis of *Angpt2* (A) or *Tek* (C) in PNETs treated as indicated (control IgG includes R.IgG, H.IgG, and R+H.IgG). Data indicate the mean fold change (±SEM) over the reference sample (control IgG) and are shown before or after normalization to mean CD31$^+$ area fraction values. Each dot represents one tumor. Statistical analysis was performed by unpaired two-tailed Student's t test.

(B) ELISA-based ANG2 protein levels in PNETs treated as indicated. Data are shown after normalization to mean vascular area fraction values. Each dot represents one tumor. Statistical analysis was performed as in (A).

(D) CD31 (green) and TIE2 (red) immunostaining and DAPI nuclear (blue) staining of PNETs treated as indicated. Scale bar, 200 μm.

(E and G) Relative area of TIE2$^+$ blood vessels (E) or hematopoietic cells (G) in PNETs treated as indicated. Each dot represents one mouse, of which multiple tumors were analyzed. Statistical analysis was performed as in (A).

(F) CD45 (green) and TIE2 (red) immunostaining of a PNET treated as indicated. The bottom-right panel shows enlargement of the inset in the bottom-left panel. Arrows indicate TEMs. Scale bar, 100 μm.

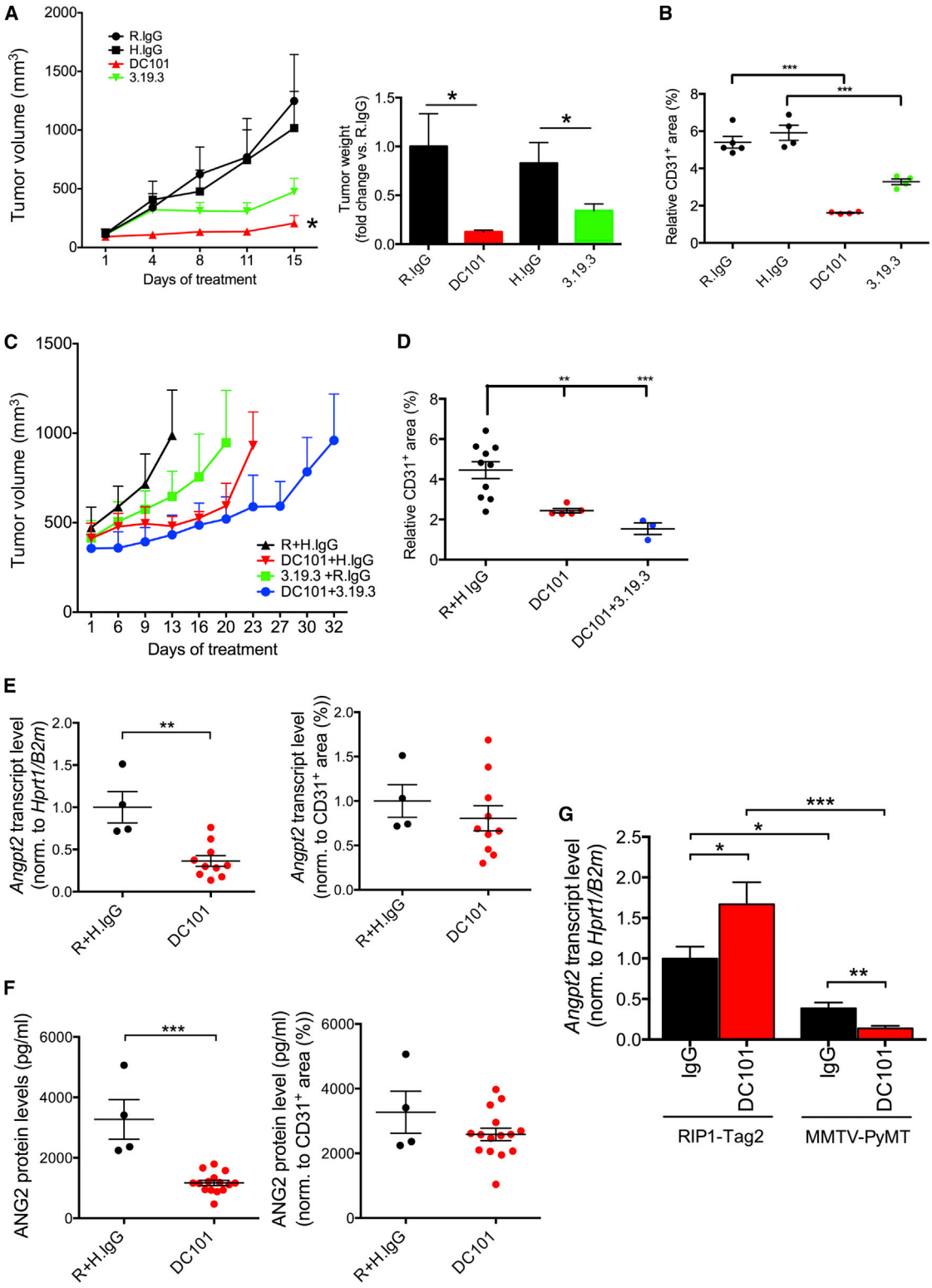

Figure 4. ANG2/VEGFR2 Blockade Does Not Upregulate *Angpt2*/ANG2 and Has Minor Additive Effects in MMTV-PyMT Mammary Tumors

(A) Left panel shows volume (mean ± SEM) of orthotopic MMTV-PyMT tumors treated as indicated: R.IgG (n = 5), H.IgG (n = 4), DC101 (n = 4), and 3.19.3 (n = 4). Right panel shows tumor weight (fold change versus R.IgG, ±SEM) at the end of the experiment. Statistical analysis was performed by unpaired two-tailed Student's t test versus the IgG control.

(legend continued on next page)

found that hypoxia upregulated *Angpt2* transcription in cultured ECs. Other cues may regulate ANG2 expression, possibly in concert with hypoxia. For example, the FOXO transcription factors can promote *ANGPT2* transcription in human ECs in response to low AKT signaling (Daly et al., 2006). VEGFA activates the phosphatidylinositol 3-kinase/AKT pathway in ECs (Claesson-Welsh and Welsh, 2013), so attenuation of AKT signaling by VEGFR2 blockade may activate *Angpt2* transcription via enhanced FOXO activity, restore AKT signaling, and promote EC survival via autocrine activation of the TIE2 receptor (Daly et al., 2013).

Tumor blood vessels typically display variegated TIE2 expression (Fathers et al., 2005; Felcht et al., 2012). Our finding of increased TIE2 expression in the blood vessels of DC101-treated tumors is intriguing. There is evidence for VEGFA signaling to directly inhibit TIE2 expression in ECs (Felcht et al., 2012), so its interception may enhance TIE2 expression. Furthermore, under the selective pressure of DC101, the growth of blood vessels that express higher TIE2 levels may be favored due to enhanced prosurvival signaling conveyed by the TIE2 receptor. Although we could not reliably assess TIE2 phosphorylation in tumor lysates (data not shown), DC101-treated PNETs upregulated the expression of both ANG2 and TIE2 in the tumor ECs, possibly reinforcing TIE2 signal transduction. On the other hand, the mammary tumors expressed lower ANG2, and DC101 did not increase its levels, hence hindering the ability of TIE2-expressing vessels to convey prosurvival and proangiogenic signals.

Late-stage RIP1-Tag2 PNETs develop resistance to VEGFA signaling blockade (Bergers and Hanahan, 2008). In agreement with previous studies by Casanovas et al. (2005), we found that a short treatment trial with DC101 substantially decreased the PNET vascular area, but consistent with the development of resistance, the tumors subsequently revascularized. It should be emphasized that, in our studies, we dosed DC101 at 0.5 mg/mouse (40 mg/kg/week), which is lower than the maximal effective (and tolerated) dose of 0.8–1.0 mg employed in other studies (Casanovas et al., 2005; Pàez-Ribes et al., 2009). Because 0.5 and 1.0 mg DC101 similarly and effectively inhibited PNET angiogenesis after a short treatment trial, 0.5 mg per mouse given biweekly might represent the optimal biological dose of DC101 in RIP1-Tag2 mice. Incidentally, the recommended effective dose of ramucirumab—a clinically approved DC101-related H.IgG1 moAb that blocks VEGFR2 (Spratlin et al., 2010)—is several times lower than that employed in our preclinical studies.

Whereas there is consensus that high doses of the multikinase inhibitor sunitinib may increase tumor invasion and metastasis, at least in mouse models of cancer (Blagoev et al., 2013; Chung et al., 2012; Ebos et al., 2009; Pàez-Ribes et al., 2009; Singh et al., 2012), the effects of specific VEGFA/VEGFR2 inhibition have been inconsistent (Chung et al., 2012; Pàez-Ribes et al., 2009; Sennino et al., 2012; Singh et al., 2012). Our findings indicate that, at a biweekly dose of 0.5 mg/mouse, DC101 does not aggravate PNET invasion and liver metastasis in RIP1-Tag2 mice. Furthermore, dual ANG2/VEGFR2 blockade blunted PNET (re)vascularization, increased hypoxia, but did not increase tumor invasion or metastasis in this mouse model. The anti-ANG2 moAb 3.19.3 potently suppresses spontaneous tumor metastasis in various mouse models of cancer (Holopainen et al., 2012; Mazzieri et al., 2011), so it is conceivable that ANG2 blockade retains its antimetastatic activity also in combination with other anticancer treatments. Because ANG2 blockade limits the proangiogenic functions of TEMs (Mazzieri et al., 2011), it is likely that the antitumoral activity of double ANG2/VEGFR2 blockade in PNETs also entails direct inhibitory effects on these perivascular macrophages.

Several ANG2-specific moAbs have been developed that are currently being evaluated in clinical trials (Eroglu et al., 2013; Gerald et al., 2013). Randomized trials of the ANG1/ANG2 bispecific peptibody AMG-386 (trebananib), in combination with chemotherapy or other antiangiogenic agents, have shown varying results (Eroglu et al., 2013: Monk et al., 2014; Peeters et al., 2013; Rini et al., 2012). Clinical studies employing ANG2-specific inhibitors are yet to be reported, and given the opposing roles of ANG1 and ANG2 in tumor angiogenesis, the clinical responses may differ from those obtained using bispecific inhibitors. ANG2 is increasingly recognized as an important molecular determinant for cancer cell metastasis (Holopainen et al., 2012; Mazzieri et al., 2011; Minami et al., 2013; Rigamonti and De Palma, 2013), so combined ANG2 and VEGFA signaling inhibition may represent a dual angioinhibitory and antimetastatic strategy that could increase the efficacy and safety of antiangiogenic therapy in cancer types that switch from a VEGF to an ANG2-dependent mode of angiogenesis.

EXPERIMENTAL PROCEDURES

Detailed methods are provided as Supplemental Experimental Procedures.

Mouse Tumor Models

FVB mice were purchased from Charles River Laboratories. Breeding pairs of transgenic C57Bl6/6J/RIP1-Tag2, C57Bl6/6J/*Rag1*$^{-/-}$/RIP1-Tag2, and FVB/MMTV-PyMT mice were donated by Douglas Hanahan and Joerg Huelsken (ISREC, EPFL). Male mice heterozygous for the oncogene were bred with

(B) Relative CD31$^+$ vascular area (mean ± SEM) of the tumors in (A). Each dot represents one tumor, of which multiple images were analyzed. Statistical analysis was performed as in (A).
(C) Volume (mean ± SEM) of tumors treated as indicated: R+H.IgG (n = 6), DC101+H.IgG (n = 5), 3.19.3+R.IgG (n = 6), and DC101+3.19.3 (n = 6). One representative experiment of two performed is shown.
(D) Relative CD31$^+$ vascular area (mean ± SEM) in tumors treated as indicated and analyzed during the resistance phase. Each dot represents one tumor, of which multiple images were analyzed. The data combine two independent experiments; tumors were analyzed either at early or late stages of the resistance phase. Statistical analysis was performed as in (A).
(E and F) qPCR-based gene expression analysis of *Angpt2* (E) or ELISA-based ANG2 protein analysis (F). Data indicate the mean fold change (±SEM) over the reference sample (R+H.IgG, for qPCR) and are shown before or after normalization to mean CD31$^+$ area fraction values. Each dot represents one tumor. The data combine two independent experiments; tumors were analyzed either at early or late stages of the resistance phase. Statistical analysis was performed as in (A).
(G) qPCR-based gene expression analysis of *Angpt2* in PNETs (IgG, n = 16; DC101, n = 15) and MMTV-PyMT carcinomas (R+H.IgG, n = 4; DC101, n = 5), shown after normalization to IgG in RIP1-Tag2 mice. Data are shown before normalization to CD31$^+$ area fraction values. Statistical analysis was performed as in (A).

wild-type females. Pups were genotyped for the SV40 large TAg (RIP1-Tag2 mice) or the Polyoma virus middle TAg (MMTV-PyMT mice) by Transnetyx (http://www.transnetyx.com). Starting from 12 weeks of age, RIP1-Tag2 mice were maintained on a sucrose-enriched diet and monitored daily. An orthotopic MMTV-PyMT tumor model was obtained by implanting dispersed tumor-derived cells from 14- to 15-week-old transgenic MMTV-PyMT mice in the fourth mammary fat pad of syngeneic (FVB) mice. All procedures were performed according to protocols approved by the Veterinary Authorities of the Canton Vaud according to the Swiss Law (licenses 2574 and 2577).

moAbs and Mouse Trials

All moAbs were provided by MedImmune and were screened for endotoxin content and activity before administration. We used the following moAbs: rat anti-mouse VEGFR2 IgG1 (DC101) at 20 mg/kg (Prewett et al., 1999); control R.IgGs at 20 mg/kg; human anti-mouse ANG2 IgG2 (3.19.3) at 10 mg/kg (Brown et al., 2010); control H.IgGs at 10 mg/kg; or their combination. The tumors (MMTV-PyMT model), pancreata, livers, and plasma (RIP1-Tag2 model) were harvested at necropsy for analysis, including (1) staining of tissue sections and analysis of vascularization, hypoxia, tumor invasion, and metastasis; (2) gene expression by qPCR; and (3) ELISA. In some experiments, before euthanasia, the mice received a systemic injection of FITC-labeled lectin (to reveal perfused blood vessels) or pimonidazole (to reveal hypoxic tissue).

Statistical Analysis

Unless indicated otherwise, values are expressed as mean ± SEM. Statistical analyses were performed by one-way ANOVA with multiple comparison Fisher's least significant difference (LSD) test or unpaired two-tailed Student's t test, as indicated in each figure panel. Detailed information is available in the Supplemental Experimental Procedures. Differences were considered statistically significant as follows: * = $0.01 \leq p < 0.05$; ** = $0.001 \leq p < 0.01$; *** = $p < 0.001$.

SUPPLEMENTAL INFORMATION

Supplemental Information includes Supplemental Experimental Procedures, four figures, and one table and can be found with this article online at http://dx.doi.org/10.1016/j.celrep.2014.06.059.

AUTHOR CONTRIBUTIONS

N.R. designed research and performed tumor studies and morphometric analyses. E.K. performed tumor studies and morphometric analyses. I.K. performed gene expression studies and ELISA. C.W.R. managed mouse colonies and performed treatment trials. C.C.L. provided moAbs and intellectual input. M.D.P. designed and supervised research, analyzed data, and wrote the paper with input from all authors.

ACKNOWLEDGMENTS

We thank Livio Trusolino, Douglas Hanahan, Donald McDonald, and Elizabeth Allen for critical discussions, Gianni Mancini (histology core facility, EPFL) for help with histology, and Giuseppe Muraca for initial assistance with mouse colonies. This work was supported by research grants from the Leenaards Foundation, the Swiss Cancer League (Oncosuisse), the European Research Council (ERC Starting grant Tie2+Monocytes), and MedImmune (to M.D.P.). C.C.L. is a MedImmune employee.

Received: December 22, 2013
Revised: May 22, 2014
Accepted: June 28, 2014
Published: July 31, 2014

REFERENCES

Allen, E., Walters, I.B., and Hanahan, D. (2011). Brivanib, a dual FGF/VEGF inhibitor, is active both first and second line against mouse pancreatic neuroendocrine tumors developing adaptive/evasive resistance to VEGF inhibition. Clin. Cancer Res. *17*, 5299–5310.

Bergers, G., and Hanahan, D. (2008). Modes of resistance to anti-angiogenic therapy. Nat. Rev. Cancer *8*, 592–603.

Blagoev, K.B., Wilkerson, J., Stein, W.D., Motzer, R.J., Bates, S.E., and Fojo, A.T. (2013). Sunitinib does not accelerate tumor growth in patients with metastatic renal cell carcinoma. Cell Reports *3*, 277–281.

Brown, J.L., Cao, Z.A., Pinzon-Ortiz, M., Kendrew, J., Reimer, C., Wen, S., Zhou, J.Q., Tabrizi, M., Emery, S., McDermott, B., et al. (2010). A human monoclonal anti-ANG2 antibody leads to broad antitumor activity in combination with VEGF inhibitors and chemotherapy agents in preclinical models. Mol. Cancer Ther. *9*, 145–156.

Casanovas, O., Hicklin, D.J., Bergers, G., and Hanahan, D. (2005). Drug resistance by evasion of antiangiogenic targeting of VEGF signaling in late-stage pancreatic islet tumors. Cancer Cell *8*, 299–309.

Chung, A.S., Lee, J., and Ferrara, N. (2010). Targeting the tumour vasculature: insights from physiological angiogenesis. Nat. Rev. Cancer *10*, 505–514.

Chung, A.S., Kowanetz, M., Wu, X., Zhuang, G., Ngu, H., Finkle, D., Komuves, L., Peale, F., and Ferrara, N. (2012). Differential drug class-specific metastatic effects following treatment with a panel of angiogenesis inhibitors. J. Pathol. *227*, 404–416.

Claesson-Welsh, L., and Welsh, M. (2013). VEGFA and tumour angiogenesis. J. Intern. Med. *273*, 114–127.

Daly, C., Pasnikowski, E., Burova, E., Wong, V., Aldrich, T.H., Griffiths, J., Ioffe, E., Daly, T.J., Fandl, J.P., Papadopoulos, N., et al. (2006). Angiopoietin-2 functions as an autocrine protective factor in stressed endothelial cells. Proc. Natl. Acad. Sci. USA *103*, 15491–15496.

Daly, C., Eichten, A., Castanaro, C., Pasnikowski, E., Adler, A., Lalani, A.S., Papadopoulos, N., Kyle, A.H., Minchinton, A.I., Yancopoulos, G.D., and Thurston, G. (2013). Angiopoietin-2 functions as a Tie2 agonist in tumor models, where it limits the effects of VEGF inhibition. Cancer Res. *73*, 108–118.

De Palma, M., and Hanahan, D. (2012). The biology of personalized cancer medicine: facing individual complexities underlying hallmark capabilities. Mol. Oncol. *6*, 111–127.

De Palma, M., and Lewis, C.E. (2013). Macrophage regulation of tumor responses to anticancer therapies. Cancer Cell *23*, 277–286.

Ebos, J.M., Lee, C.R., Cruz-Munoz, W., Bjarnason, G.A., Christensen, J.G., and Kerbel, R.S. (2009). Accelerated metastasis after short-term treatment with a potent inhibitor of tumor angiogenesis. Cancer Cell *15*, 232–239.

Eklund, L., and Saharinen, P. (2013). Angiopoietin signaling in the vasculature. Exp. Cell Res. *319*, 1271–1280.

Eroglu, Z., Stein, C.A., and Pal, S.K. (2013). Targeting angiopoietin-2 signaling in cancer therapy. Expert Opin. Investig. Drugs *22*, 813–825.

Fathers, K.E., Stone, C.M., Minhas, K., Marriott, J.J., Greenwood, J.D., Dumont, D.J., and Coomber, B.L. (2005). Heterogeneity of Tie2 expression in tumor microcirculation: influence of cancer type, implantation site, and response to therapy. Am. J. Pathol. *167*, 1753–1762.

Felcht, M., Luck, R., Schering, A., Seidel, P., Srivastava, K., Hu, J., Bartol, A., Kienast, Y., Vettel, C., Loos, E.K., et al. (2012). Angiopoietin-2 differentially regulates angiogenesis through TIE2 and integrin signaling. J. Clin. Invest. *122*, 1991–2005.

Ferrara, N. (2010). Role of myeloid cells in vascular endothelial growth factor-independent tumor angiogenesis. Curr. Opin. Hematol. *17*, 219–224.

Gabrusiewicz, K., Liu, D., Cortes-Santiago, N., Hossain, M.B., Conrad, C.A., Aldape, K.D., Fuller, G.N., Marini, F.C., Alonso, M.M., Idoate, M.A., et al. (2014). Anti-vascular endothelial growth factor therapy-induced glioma invasion is associated with accumulation of Tie2-expressing monocytes. Oncotarget *5*, 2208–2220.

Gerald, D., Chintharlapalli, S., Augustin, H.G., and Benjamin, L.E. (2013). Angiopoietin-2: an attractive target for improved antiangiogenic tumor therapy. Cancer Res. *73*, 1649–1657.

Goede, V., Coutelle, O., Neuneier, J., Reinacher-Schick, A., Schnell, R., Koslowsky, T.C., Weihrauch, M.R., Cremer, B., Kashkar, H., Odenthal, M., et al. (2010). Identification of serum angiopoietin-2 as a biomarker for clinical outcome of colorectal cancer patients treated with bevacizumab-containing therapy. Br. J. Cancer *103*, 1407–1414.

Hashizume, H., Falcón, B.L., Kuroda, T., Baluk, P., Coxon, A., Yu, D., Bready, J.V., Oliner, J.D., and McDonald, D.M. (2010). Complementary actions of inhibitors of angiopoietin-2 and VEGF on tumor angiogenesis and growth. Cancer Res. *70*, 2213–2223.

Helfrich, I., Edler, L., Sucker, A., Thomas, M., Christian, S., Schadendorf, D., and Augustin, H.G. (2009). Angiopoietin-2 levels are associated with disease progression in metastatic malignant melanoma. Clin. Cancer Res. *15*, 1384–1392.

Holopainen, T., Saharinen, P., D'Amico, G., Lampinen, A., Eklund, L., Sormunen, R., Anisimov, A., Zarkada, G., Lohela, M., Heloterä, H., et al. (2012). Effects of angiopoietin-2-blocking antibody on endothelial cell-cell junctions and lung metastasis. J. Natl. Cancer Inst. *104*, 461–475.

Huang, H., Lai, J.Y., Do, J., Liu, D., Li, L., Del Rosario, J., Doppalapudi, V.R., Pirie-Shepherd, S., Levin, N., Bradshaw, C., et al. (2011). Specifically targeting angiopoietin-2 inhibits angiogenesis, Tie2-expressing monocyte infiltration, and tumor growth. Clin. Cancer Res. *17*, 1001–1011.

Kienast, Y., Klein, C., Scheuer, W., Raemsch, R., Lorenzon, E., Bernicke, D., Herting, F., Yu, S., The, H.H., Martarello, L., et al. (2013). Ang-2-VEGF-A CrossMab, a novel bispecific human IgG1 antibody blocking VEGF-A and Ang-2 functions simultaneously, mediates potent antitumor, antiangiogenic, and antimetastatic efficacy. Clin. Cancer Res. *19*, 6730–6740.

Kim, S., Dobi, E., Jary, M., Monnien, F., Curtit, E., Nguyen, T., Lakkis, Z., Heyd, B., Fratte, S., Cléau, D., et al. (2013). Bifractionated CPT-11 with LV5FU2 infusion (FOLFIRI-3) in combination with bevacizumab: clinical outcomes in first-line metastatic colorectal cancers according to plasma angiopoietin-2 levels. BMC Cancer *13*, 611.

Leow, C.C., Coffman, K., Inigo, I., Breen, S., Czapiga, M., Soukharev, S., Gingles, N., Peterson, N., Fazenbaker, C., Woods, R., et al. (2012). MEDI3617, a human anti-angiopoietin 2 monoclonal antibody, inhibits angiogenesis and tumor growth in human tumor xenograft models. Int. J. Oncol. *40*, 1321–1330.

Mazzieri, R., Pucci, F., Moi, D., Zonari, E., Ranghetti, A., Berti, A., Politi, L.S., Gentner, B., Brown, J.L., Naldini, L., and De Palma, M. (2011). Targeting the ANG2/TIE2 axis inhibits tumor growth and metastasis by impairing angiogenesis and disabling rebounds of proangiogenic myeloid cells. Cancer Cell *19*, 512–526.

Minami, T., Jiang, S., Schadler, K., Suehiro, J., Osawa, T., Oike, Y., Miura, M., Naito, M., Kodama, T., and Ryeom, S. (2013). The calcineurin-NFAT-angiopoietin-2 signaling axis in lung endothelium is critical for the establishment of lung metastases. Cell Reports *4*, 709–723.

Monk, B.J., Poveda, A., Vergote, I., Raspagliesi, F., Fujiwara, K., Bae, D.S., Oaknin, A., Ray-Coquard, I., Provencher, D.M., Karlan, B.Y., et al. (2014). Anti-angiopoietin therapy with trebananib for recurrent ovarian cancer (TRINOVA-1): a randomised, multicentre, double-blind, placebo-controlled phase 3 trial. Lancet Oncol. *15*, 799–808.

Oh, H., Takagi, H., Suzuma, K., Otani, A., Matsumura, M., and Honda, Y. (1999). Hypoxia and vascular endothelial growth factor selectively up-regulate angiopoietin-2 in bovine microvascular endothelial cells. J. Biol. Chem. *274*, 15732–15739.

Pàez-Ribes, M., Allen, E., Hudock, J., Takeda, T., Okuyama, H., Viñals, F., Inoue, M., Bergers, G., Hanahan, D., and Casanovas, O. (2009). Antiangiogenic therapy elicits malignant progression of tumors to increased local invasion and distant metastasis. Cancer Cell *15*, 220–231.

Park, J.H., Park, K.J., Kim, Y.S., Sheen, S.S., Lee, K.S., Lee, H.N., Oh, Y.J., and Hwang, S.C. (2007). Serum angiopoietin-2 as a clinical marker for lung cancer. Chest *132*, 200–206.

Peeters, M., Strickland, A.H., Lichinitser, M., Suresh, A.V., Manikhas, G., Shapiro, J., Rogowski, W., Huang, X., Wu, B., Warner, D., et al. (2013). A randomised, double-blind, placebo-controlled phase 2 study of trebananib (AMG 386) in combination with FOLFIRI in patients with previously treated metastatic colorectal carcinoma. Br. J. Cancer *108*, 503–511.

Prewett, M., Huber, J., Li, Y., Santiago, A., O'Connor, W., King, K., Overholser, J., Hooper, A., Pytowski, B., Witte, L., et al. (1999). Antivascular endothelial growth factor receptor (fetal liver kinase 1) monoclonal antibody inhibits tumor angiogenesis and growth of several mouse and human tumors. Cancer Res. *59*, 5209–5218.

Rigamonti, N., and De Palma, M. (2013). A role for angiopoietin-2 in organ-specific metastasis. Cell Reports *4*, 621–623.

Rini, B., Szczylik, C., Tannir, N.M., Koralewski, P., Tomczak, P., Deptala, A., Dirix, L.Y., Fishman, M., Ramlau, R., Ravaud, A., et al. (2012). AMG 386 in combination with sorafenib in patients with metastatic clear cell carcinoma of the kidney: a randomized, double-blind, placebo-controlled, phase 2 study. Cancer *118*, 6152–6161.

Rivera, L., Pandika, M., and Bergers, G. (2014). Escape mechanisms from anti-angiogenic therapy: an immune cell's perspective. Adv. Exp. Med. Biol. *772*, 83–99.

Sennino, B., and McDonald, D.M. (2012). Controlling escape from angiogenesis inhibitors. Nat. Rev. Cancer *12*, 699–709.

Sennino, B., Ishiguro-Oonuma, T., Wei, Y., Naylor, R.M., Williamson, C.W., Bhagwandin, V., Tabruyn, S.P., You, W.K., Chapman, H.A., Christensen, J.G., et al. (2012). Suppression of tumor invasion and metastasis by concurrent inhibition of c-Met and VEGF signaling in pancreatic neuroendocrine tumors. Cancer Discov. *2*, 270–287.

Shojaei, F., Singh, M., Thompson, J.D., and Ferrara, N. (2008). Role of Bv8 in neutrophil-dependent angiogenesis in a transgenic model of cancer progression. Proc. Natl. Acad. Sci. USA *105*, 2640–2645.

Singh, M., Couto, S.S., Forrest, W.F., Lima, A., Cheng, J.H., Molina, R., Long, J.E., Hamilton, P., McNutt, A., Kasman, I., et al. (2012). Anti-VEGF antibody therapy does not promote metastasis in genetically engineered mouse tumour models. J. Pathol. *227*, 417–430.

Spratlin, J.L., Cohen, R.B., Eadens, M., Gore, L., Camidge, D.R., Diab, S., Leong, S., O'Bryant, C., Chow, L.Q., Serkova, N.J., et al. (2010). Phase I pharmacologic and biologic study of ramucirumab (IMC-1121B), a fully human immunoglobulin G1 monoclonal antibody targeting the vascular endothelial growth factor receptor-2. J. Clin. Oncol. *28*, 780–787.

Van der Veldt, A.A., Lubberink, M., Bahce, I., Walraven, M., de Boer, M.P., Greuter, H.N., Hendrikse, N.H., Eriksson, J., Windhorst, A.D., Postmus, P.E., et al. (2012). Rapid decrease in delivery of chemotherapy to tumors after anti-VEGF therapy: implications for scheduling of anti-angiogenic drugs. Cancer Cell *21*, 82–91.

Vasudev, N.S., and Reynolds, A.R. (2014). Anti-angiogenic therapy for cancer: current progress, unresolved questions and future directions. Angiogenesis *17*, 471–494.

Willett, C.G., Boucher, Y., di Tomaso, E., Duda, D.G., Munn, L.L., Tong, R.T., Chung, D.C., Sahani, D.V., Kalva, S.P., Kozin, S.V., et al. (2004). Direct evidence that the VEGF-specific antibody bevacizumab has antivascular effects in human rectal cancer. Nat. Med. *10*, 145–147.

Yang, J.C., Haworth, L., Sherry, R.M., Hwu, P., Schwartzentruber, D.J., Topalian, S.L., Steinberg, S.M., Chen, H.X., and Rosenberg, S.A. (2003). A randomized trial of bevacizumab, an anti-vascular endothelial growth factor antibody, for metastatic renal cancer. N. Engl. J. Med. *349*, 427–434.

Yoon, S.S., Duda, D.G., Karl, D.L., Kim, T.M., Kambadakone, A.R., Chen, Y.L., Rothrock, C., Rosenberg, A.E., Nielsen, G.P., Kirsch, D.G., et al. (2011). Phase II study of neoadjuvant bevacizumab and radiotherapy for resectable soft tissue sarcomas. Int. J. Radiat. Oncol. Biol. Phys. *81*, 1081–1090.